



Article

Evaluating the Impact of DEM Spatial Resolution on 3D Rockfall Simulation in GIS Environment

Maria P. Kakavas ^{1,*}, Paolo Frattini ², Alberto Previati ² and Konstantinos G. Nikolakopoulos ¹

¹ Department of Geology, Division of Applied Geology and Geophysics, University of Patras, 26504 Patras, Greece; knikolakop@upatras.gr

² Department of Earth and Environmental Science, Universita degli Studi di Milano-Bicocca, 20126 Milan, Italy; paolo.frattini@unimib.it (P.F.); alberto.previati@unimib.it (A.P.)

* Correspondence: kakava.maria@upatras.gr

Abstract: Rockfalls are natural geological phenomena characterized by the abrupt detachment and freefall descent of rock fragments from steep slopes. These events exhibit considerable variability in scale, velocity, and trajectory, influenced by the geological composition of the slope, the topography, and other environmental conditions. By employing advanced modeling techniques and terrain analysis, researchers aim to predict and control rockfall hazards to prevent casualties and protect properties in areas at risk. In this study, two rockfall events in the villages of Mylooi and Platiana of Ilia prefecture were examined. The research was conducted by means of HY-STONE software, which performs 3D numerical modeling of the motion of non-interacting blocks. To perform this modeling, input files require the processing of base maps and datasets in a GIS environment. Stochastic modeling and 3D descriptions of slope topography, based on Digital Elevation Models (DEMs) without spatial resolution limitations, ensure multiscale analysis capabilities. Considering this capability, seven freely available DEMs, derived from various sources, were applied in HY-STONE with the scope of performing a large number of multiparametric analyses and selecting the most appropriate and efficient DEM for the software requirements. All the necessary data for the multiparametric analyses were generated within a GIS environment, utilizing either the same restitution coefficients and rolling friction coefficient or varying ones. The results indicate that finer-resolution DEMs capture detailed terrain features, enabling the precise identification of rockfall source areas and an accurate depiction of the kinetic energy distribution. Further, the results show that a correct application of the model to different DEMs requires a specific parametrization to account for the different roughness of the models.



Citation: Kakavas, M.P.; Frattini, P.; Previati, A.; Nikolakopoulos, K.G. Evaluating the Impact of DEM Spatial Resolution on 3D Rockfall Simulation in GIS Environment. *Geosciences* **2024**, *14*, 200. <https://doi.org/10.3390/geosciences14080200>

Academic Editor: Mimmo Palano

Received: 4 June 2024

Revised: 12 July 2024

Accepted: 24 July 2024

Published: 29 July 2024



Copyright: © 2024 by the authors. Licensee MDPI, Basel, Switzerland. This article is an open access article distributed under the terms and conditions of the Creative Commons Attribution (CC BY) license (<https://creativecommons.org/licenses/by/4.0/>).

1. Introduction

Estimating a rockfall risk, a process that involves risk assessment, susceptibility modeling, and delineating hazard zones, represents a challenging endeavor in rockfall research [1]. A variety of methods have been developed recently, with many focused on measuring the rockfall's intensity, identifying specific areas of concern, and determining the frequency of rockfall occurrences [2]. The complexity of rockfall risk analysis, which necessitates multiscale approaches, has led to the integration of various disciplines and techniques. Remote sensing, in particular, has proven to be a useful tool in rockfall investigations, providing precise models of potential hazard areas and capturing intricate details such as the lithological composition and angles of slopes and source zones [3]. These capabilities are essential, particularly because many hazardous rock slopes are inaccessible, where crucial data can only be obtained via remote sensing techniques. Slope characteristics play a critical role in rockfall hazard assessments, as they significantly influence both the initiation and behavior of rockfalls [4,5]. Digital Elevation Models (DEMs) are utilized to extract slope data and topographical parameters, which are essential for assessing and

categorizing these geological features. One of the most beneficial features of DEMs is their capacity to support the generation, analysis, and mapping of slope parameters through Geographic Information System (GIS) tools [5]. The spatial resolutions of DEMs are a crucial aspect in rockfall simulations: lower-resolution DEMs tend to oversimplify the terrain's roughness, thereby reducing the accuracy of the predicted rockfall areas [6]; conversely, higher-resolution DEMs typically provide more detailed results for various rockfall-related factors [7]. Consequently, DEMs of varying resolutions are incorporated into numerous rockfall simulation software to meet the diverse requirements of rockfall analysis [8–19].

A variety of software has been developed to facilitate two-dimensional (2D) and three-dimensional (3D) rockfall trajectory simulations using DEMs. Currently, the accuracy of trajectory calculations has reached a high level due to advancements in numerical simulation techniques [20]. A notable example of such software is RocFall, developed by Stevens, W.D. (1998), which is recognized for its capability to calibrate various slope materials. In this process, DEMs indirectly contribute by providing slope profiles [21,22]. In RocFall, the spatial resolution plays a critical role in the simulations, where smaller cell sizes result in increased bounce heights and kinetic energies [23]. Recent studies involving seven different spatial resolutions ranging from 0.05 m to 90 m have shown that only those with higher pixel sizes can produce realistic trajectories [24]. Rotomap, another model that uses the lumped-mass approach, illustrates how higher-accuracy DEMs more accurately reflect the actual rockfall trajectories [25]. Furthermore, the impact of DEM spatial resolution on rockfall modeling has been explored through the empirical model CONEFALL, which has proven most effective for regional-scale studies [26]. Testing various spatial resolutions within this software has shown that DEMs with 1 m and 5 m resolutions are suitable for small-scale rockfall events, while those with 12.5 m and 25 m are better suited for larger scales. However, DEMs with a 100 m resolution are found to be unsuitable for such studies due to their low accuracy [26].

Conversely, STONE is a lumped-mass 3D rockfall simulation software that directly utilizes DEMs to model topography in raster format [27]. Renowned for its capability to simulate rockfall trajectories, STONE stands out due to its algorithm's ability to operate without the constraints of spatial resolution [28,29]. In conducting hazard assessments for both regional and large-scale events, STONE applies resampling techniques to DEMs, demonstrating that finer resolutions provide more detailed and accurate simulations of rockfall trajectories [28]. Furthermore, the precision of DEMs in STONE significantly influences the lateral dispersion, particularly noting an increase in dispersion with finer resolutions on slopes angled at 45 degrees [30]. Meanwhile, in the RAMMS software, although cell size does not influence the outcomes in flatter terrains, it is crucial in rough terrains where fine-resolution DEMs are recommended for accurately depicting terrain irregularities [31].

HY-STONE is another software designed for the 3D numerical modeling of rockfall processes. It simulates the trajectory of non-interacting blocks through various stages, including free fall, impact, and rolling, with a hybrid approach [30,32,33]. Notable features of HY-STONE include its ability to utilize a 3D vector representation of slope topography derived from raster Digital Elevation Models (DEMs), along with its compatibility with both raster and vector ArcGIS formats [27,34,35]. The software uses three coefficients (two restitution coefficients, normal and tangential, and a rolling friction coefficient), which are spatially described according to the DEM's accuracy by demonstrating that simulated runout distance increases as the DEM's resolution decreases [36,37]. A calibration process of the coefficients is therefore necessary [38].

The main objective of this study is to assess how the DEM's cell size impacts the rockfall data generated by the HY-STONE software, given that the spatial resolution of DEMs significantly influences the rockfall simulation process. Secondly, the paper aims to investigate the effect of the resolution on the calibration of model parameters. This research employs HY-STONE to analyze two rockfall events in Western Greece, specifically in the Myloai and Platiana settlements of the Peloponnese region. The goal is to determine

how the accuracy of various DEMs affects the software's output and to validate these results with field observations. To this end, seven freely available DEMs (with spatial resolutions ranging from 5 cm to 90 m) are utilized, including the UAV DEM, DEM from the Greek Cadastral, ALOS AW3D30 DEM, ASTER GDEM, SRTM30 DEM, SRTM90 DEM, and TanDEM_X, to explore their effects on the modeling outcomes.

2. Software and Materials

HY-STONE is a software developed for 3D numerical modeling of rockfall processes, including the simulation of the motion of non-interacting blocks, utilizing a high-resolution 3D description of slope geometry for accurate multiscale stochastic modeling [30,32,33]. It is capable of modeling the free fall, impact, and rolling of blocks, with energy loss simulations upon impact or by rolling based on a hybrid (cinematic and dynamic) approach. It exports the results as raster grids and vector files, detailing the frequency of rockfall, fly height, velocity, kinetic energy, and information on each simulated block's kinematics and dynamics.

The software features a 3D vector description of slope topography by means of a vector triangular network (TRN) obtained from a raster DEM [27,34]. The TRN offers a continuous description of the topography by transforming the DEM's grid points into vertices of a network of contiguous, non-overlapping triangles. In the XYZ global (inertial) Cartesian system, the 3D space is defined by the orthogonal axes X, Y, and Z, where Z represents the elevation. The xp, yp, and zp local (triangle) in the Cartesian system are positioned within this global context, oriented on each triangle's plane, allowing for localized terrain descriptions on the triangle's surface. In the context of rockfall simulation, the software uses the normals to the triangles to compute the angles of impact and to adjust the trajectory of rock blocks upon collision with the ground.

Furthermore, HY-STONE takes into account the slope's lithology, land use, and roughness to inform the rolling friction coefficient ($\tan\Phi_r$, named A_T in this work), as well as the normal (E_N) and tangential (E_T) restitution coefficients that control energy loss upon impact. These coefficients are derived from the literature or experience and can be calibrated against field observations. In particular, E_N and E_T are essential for managing the energy dissipation of blocks, influenced by factors that include the type of surface lithology and the existing vegetation or land use patterns. The coefficients range from 0 (indicating no restitution) to 1 (indicating complete restitution). In the GIS, raster datasets are typically produced by first reclassifying maps of "unique condition units," which are areas defined by specific environmental characteristics such as lithology and vegetation or land use. These maps are then transformed into a raster format. The initial values are typically sourced from scholarly literature and subsequently fine-tuned through multiple simulation iterations to ensure they match well with the field observations, including historical and experimental data. The third coefficient (A_T), which determines the energy dissipated as blocks roll over the slope's surface, depends on various attributes such as surface lithology, land use, and surface roughness. This coefficient is typically a positive floating number between 0 and 1 and is assigned to each model cell. These data are also generated by reclassifying unique condition unit maps and necessitating calibration through iterative simulations to ensure precision and reliability in the modeling outcomes.

For the stochastic simulation, a normal distribution is used to simulate the natural variability of the restitution and friction coefficients within $\pm 30\%$ and 20% of their initial values, respectively. These specific distributions are chosen to realistically represent the variability and uncertainty inherent in natural rockfall events, enhancing the predictive accuracy of the simulations.

In summary, the software requires five spatially distributed input data, provided as ASCII raster files in the ESRI GridAscii format as follows: (i) DEM, (ii) rockfall source locations, (iii) normal (E_N) restitution coefficients, (iv) tangential (E_T) restitution coefficients, and (v) the rolling friction coefficient (A_T).

This study applies HY-STONE to execute a series of analyses, repeated seven times using DEMs of varying accuracies, aiming to conclude the most appropriate one for rockfall simulation. The resolutions explored include a 0.05 m spatial resolution UAV DEM generated from field surveys, a 5 m resolution DEM from the Greek Cadastral, three 30 m resolution DEMs (ALOS AW3D30 DEM, ASTER GDEM, and SRTM30 DEM), and two 90 m resolution DEMs (SRTM90 DEM and TanDEM_X). Two well-known rockfall events in the villages of Mylooi and Platiana of Ilia prefecture were examined (Figure 1).

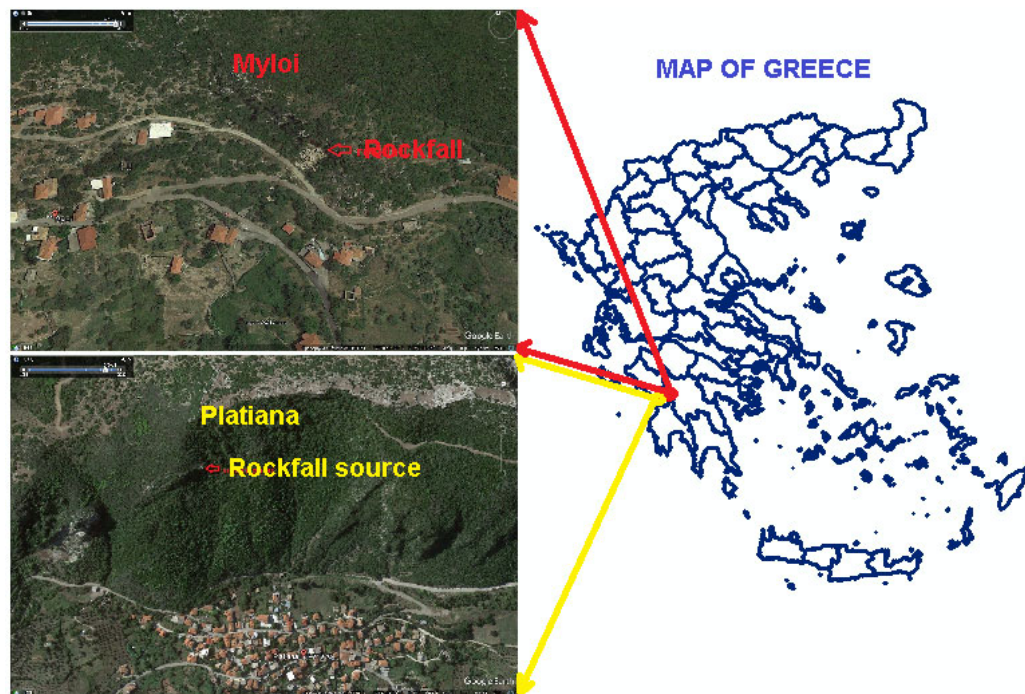


Figure 1. Pictures of the rockfall events in the Mylooi and Platiana region in relation to the Hellenic region.

3. Study Areas

3.1. Mylooi Settlement

Located in the Ilia prefecture of Western Greece's Peloponnese region, the village of Mylooi is geologically situated within the Olonos-Pindos and Gavrovo-Tripolis geotectonic units. According to the engineering geological map of Greece provided by the Hellenic Survey of Geology and Mineral Exploration (HSGME), the area predominantly consists of Upper Cretaceous limestones. The mountainous terrain above the Mylooi settlement is characterized by extensive areas of barren limestones and cherts. Research by Depountis et al. (2010) indicates that the predominant fault orientations in the region are east–west (E–W) and northeast–southwest (NE–SW) [39]. Certain weathering processes have significantly weakened the cohesion of the underlying limestone, leading to the detachment of rock blocks and the occurrence of rock sliding. These geological formations are characterized by a slope angle ranging from 45 to 60 degrees [40]. Additionally, the Ilia prefecture experienced devastating wildfires in August 2007, which obliterated the vegetation across approximately 870 km² of forested and agricultural land. This extreme event resulted in over sixty fatalities, hundreds of injuries, and extensive damage. The loss of vegetation, compounded by heavy rainfall, reactivated the mechanisms responsible for various scales of rockfall events. Despite the authorities designating the broader Mylooi area as reforestable land, a significant rockfall occurred near Andritsaina town on 26 January 2019. This event was triggered by the combined effects of intense rainfall and the complete absence of a root system, which led to weathering and subsequent loss of cohesion. As a result, detached boulders rolled down the slope, causing substantial damage to two houses and blocking

the main roads at the village entrance (Figure 2). The slope fragments displaced onto the road and at the end of the slope profile were estimated to have a total volume of 147 m^3 .



Figure 2. Pictures of the rockfall in the Mylooi region illustrate the final position of rock blocks. Red arrows indicate the final positions of the rock masses at the conclusion of the rockfall event.

3.2. Platiana Settlement

Similar to Mylooi, Platiana is another village in the Ilia prefecture of Peloponnese, located approximately 25 km from Mylooi (Figure 3). The surrounding area is primarily composed of Upper Cretaceous limestones, as indicated by the engineering geological map of Greece, and is part of the Pindos geotectonic unit according to the Hellenic Survey of Geology and Mineral Exploration (HSGME). This region is a segment of the broader Pindic Unit that has been thrust westward. Near the settlement, there are significant outcrops of limestone with varying thicknesses from thin to medium layers. According to Vagenas (2020) [40], these limestone layers are locally intercalated with chert layers.

Platiana, like Mylooi, experienced the devastating wildfires of 2007 and has been declared reforestable land over the past decade. Following the natural reforestation efforts, the vegetation levels have been fully restored (Figure 4). However, from 2008 to 2018, the mountain slopes adjacent to Platiana were completely barren. Similar to other cases, the lack of vegetation exposed the slopes to corrosion factors that compromised their structural integrity and triggered the release of internal stresses. As a result, rocks of various sizes became detached from the main body and collapsed. Notably, on 4 December 2018, after heavy rainfall, a massive boulder, approximately 10 m^3 in volume, slid down the slope. Fortunately, it came to a stop in a churchyard, causing no casualties. During its downward course, the boulder penetrated two dry stone walls that served as field boundaries (Figure 3).

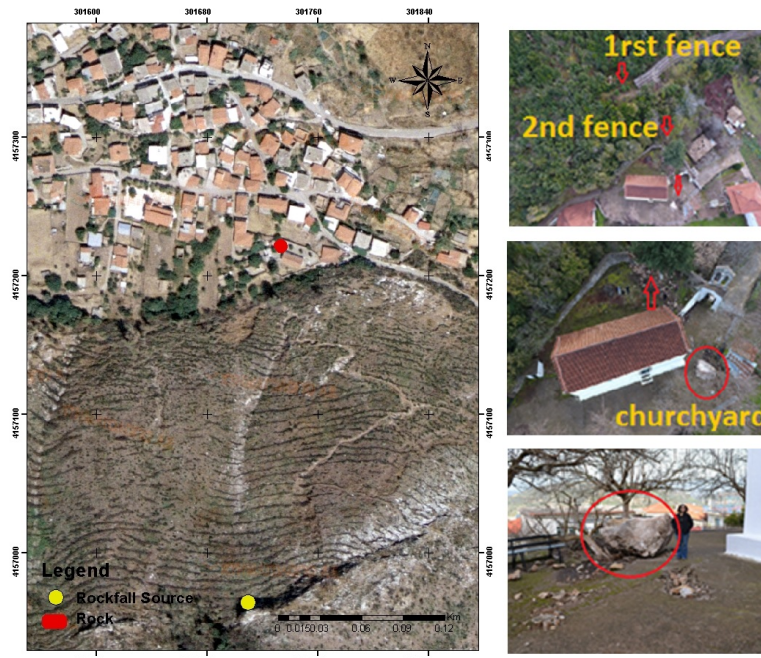


Figure 3. Picture taken from the Platiana region after the rockfall event. The slope picture is taken from the Greek Cadastral (2008).



Figure 4. Reforestation procedures in the slope next to the Platiana village. The slope pictures are taken from the Greek Cadastral.

4. Results

In this section, the results of the rockfall simulations through HY-STONE software are presented. Two different methods were accomplished; the first method is by using the rockfall simulations with DEMs of various resolutions—the same restitution coefficients (E_N and E_T) and rolling friction coefficient (A_T) calibrated for the highest resolution DEM. The second method consisted of adjusting the parameters to calibrate the model to each resolution in order to study the variations of calibrated coefficients as a function of the DEM's resolution.

4.1. Results by Using the Same Restitution Coefficients and Rolling Friction Coefficient

4.1.1. Mylo Rockfall

HY-STONE utilizes spatially distributed data for rockfall modeling, which involves accurately mapping topography, identifying rockfall sources, and evaluating the slope surface characteristics related to energy dissipation from block impacts and rolling. Additionally, detailed information on the geometry of falling blocks, such as their shape and size, along with the initial conditions and algorithm settings, is essential. To achieve this, seven DEMs were used, including the UAV DEM, DEM from the Greek Cadastral, ALOS

AW3D30 DEM, ASTER GDEM, SRTM30 DEM, SRTM90 DEM, and TanDEM_X, spanning resolutions from 0.3 m to 90 m to provide a precise topographical representation.

Given the extensive tree coverage, the UAV's original DSM underwent processing in Cloud Compare Software to manually remove vegetation, obtaining the UAV DEM. This is a necessary step before conducting a HY-STONE simulation because trees may be interpreted as barriers [33]. Specifically, Figure 5 provides the differences in vegetation coverage before (left image) and after (right image) the procedure in the Cloud Compare Software. The left image shows the landscape with full vegetation, where the dense canopy masks the underlying ground features. After processing, the right image shows some residual green areas, which are actually areas where the vegetation density was difficult to resolve completely using the software; however, these might be shadows and low-lying shrubs that remain post-processing. What might seem like gaps in the right image are actually areas where the vegetation has been effectively removed.

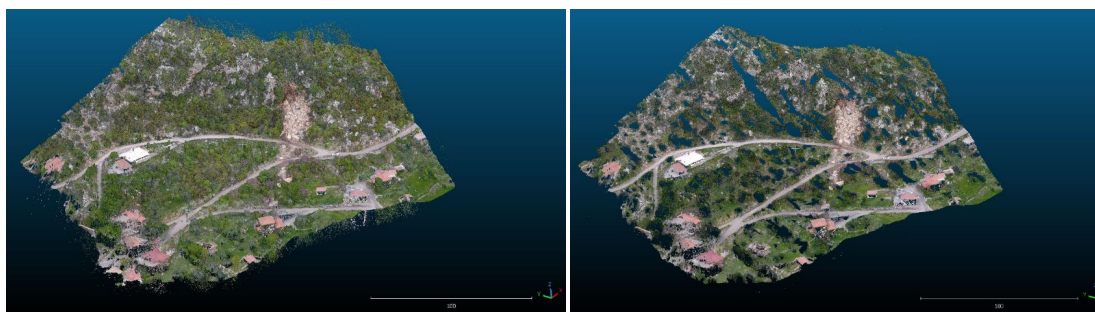


Figure 5. Mylooi area before (left image) and after (right image) removing the vegetation through Cloud Compare Software.

The restitution coefficients, E_N and E_T , along with the rolling friction coefficient A_T , were established through back-calibration on the highest resolution DEM, based on the 2018 rockfall event (Table 1).

Table 1. Coefficients of restitution and rolling friction in Mylooi rockfall, calibrated on the UAV DEM.

Description	E_N	E_T	A_T
Houses	0.20	0.20	1.00
Road-asphalt	0.55	0.75	0.37
Debris well vegetated	0.35	0.60	0.55
Debris without vegetation	0.40	0.65	0.42

Given that HY-STONE operates on a stochastic model, simulations were performed with 3000 rocks to provide a more accurate representation of the rockfall dynamics. The outcomes of the HY-STONE analysis for the Mylooi rockfall are displayed in terms of transit frequency. The following maps (Figure 6) illustrate the cumulative count of rockfall trajectories that pass through each model cell.

Figure 6a, derived from the UAV DEM, illustrates the areas of high transit frequency predominantly in the central sections of the rockfall's left and right flanks. Moving outward from the central rockfall mass, the transit frequency gradually diminishes to zero towards the periphery. This pattern aligns with the actual conditions observed on-site, where the bulk of the rockfall material halted in the high transit zones while only a few scattered blocks reached the outer edges.

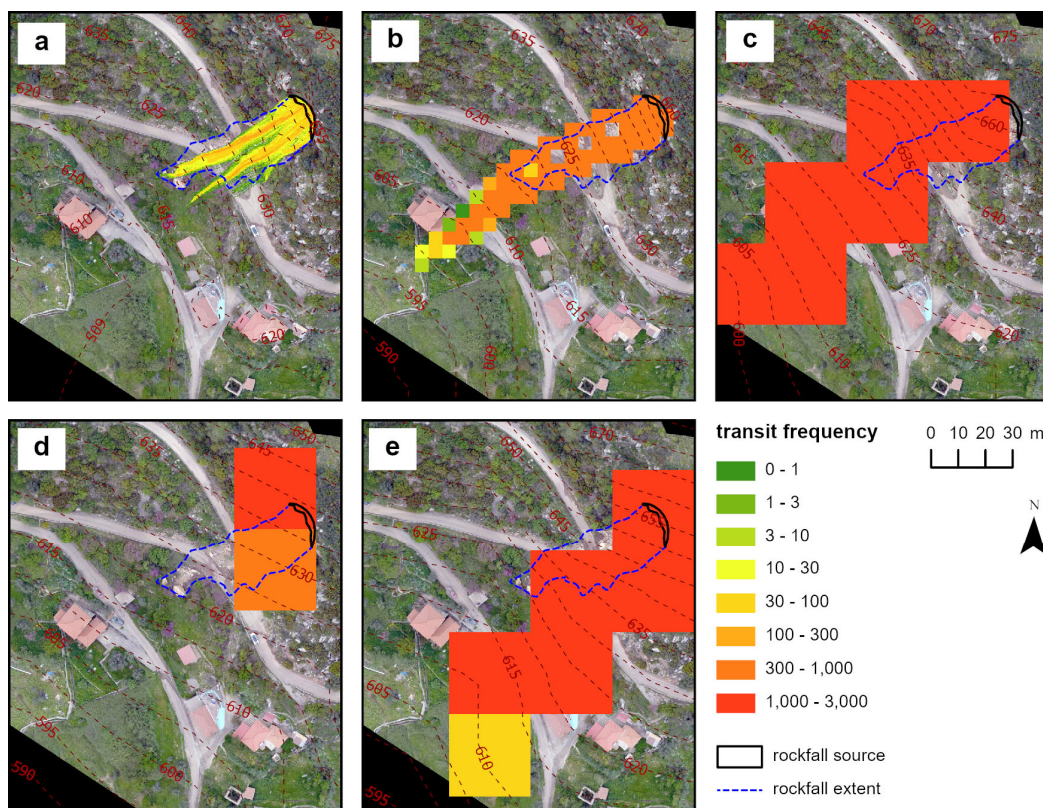


Figure 6. HY-STONE results for the site of Myloai using parameters (E_N , E_T , and A_T) calibrated on the UAV DEM. The transit frequencies of blocks are shown for (a) UAV DEM, (b) Greek Cadastral DEM, (c) ALOS AW3D30 DEM, (d) ASTER GDEM, and (e) SRTM30 DEM.

The result from using the Greek Cadastral DEM, depicted in Figure 6b, shows that the rock movement ceased around the houses, where the transit frequency values were observed to be medium to low.

The simulations using the ALOS AW3D30 DEM, ASTER GDEM, and SRTM30 DEM (Figure 6c–e) show a distinct distribution of only high or low frequencies without intermediate values. Given the small scale of the Myloai rockfall event (about 30 m of maximum runout), the 30 m resolution DEMs do not yield reliable results. Consequently, the SRTM90 DEM and TanDEM_X, with their coarser resolution, are deemed unsuitable for modeling rockfalls of this particular magnitude, and therefore, simulations using these DEMs were not performed.

The software also produces output files labeled min-ecv.asc, med-ecv.asc, and max-ecv.asc (and optionally, min-ecv.img, med-ecv.img, and max-ecv.img), which represent the minimum, average, and maximum translational kinetic energy of the blocks, respectively, calculated for each model cell in Joules (J). Subsequently, the maximum translational kinetic energies for the Myloai rockfall are presented in kJ in Figure 7a–e.

Figure 7a illustrates the calculated maximum translational kinetic energy using the UAV DEM, which estimates this energy as ranging from 0 to 500 kJ. The highest energy levels were recorded in the central mass of the rockfall, while lower energy levels were observed at the periphery. The energy simulation ceases at the points where the rock movement stops. The Greek Cadastral DEM displays maximum kinetic energies with values of 0 J at the rockfall source and significantly higher values ranging from 200–500 kJ on the right side of the rockfall mass (Figure 7b). Similar kinetic energy ranges are depicted in the simulations using the ALOS AW3D30 DEM and SRTM30 DEM (Figure 7c,e), showing small ranges of variation. Conversely, the ASTER GDEM registered very low values of maximum kinetic energies, not exceeding 10 kJ (Figure 7d).

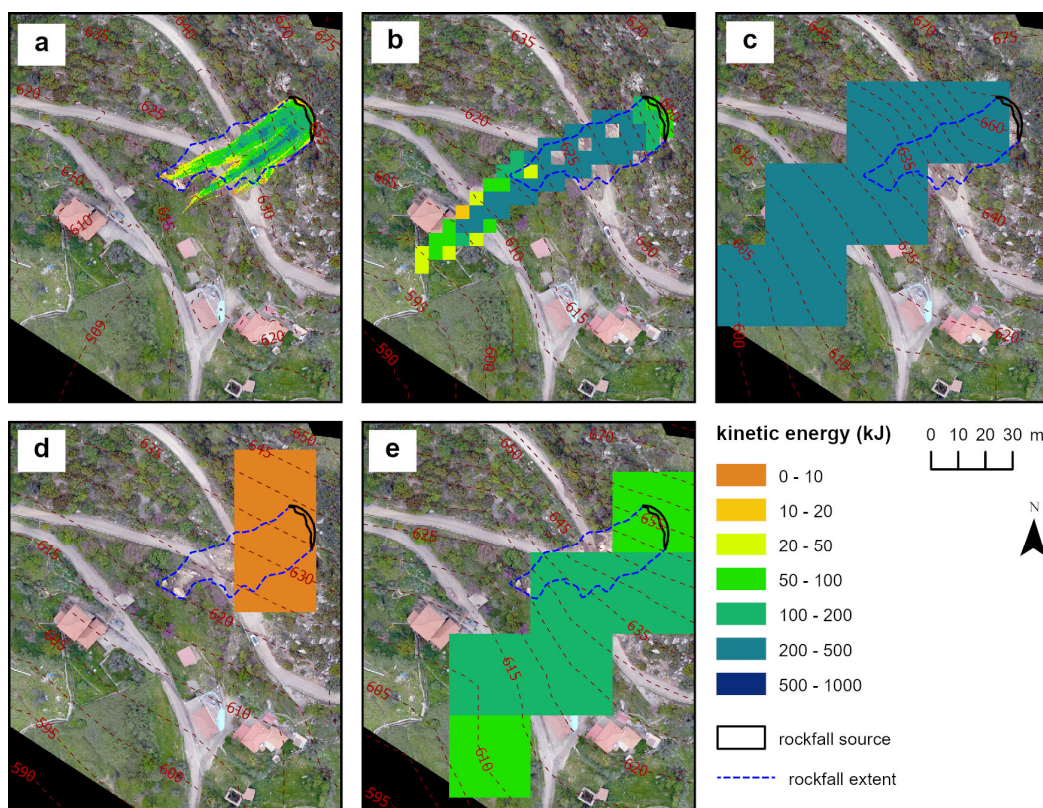


Figure 7. HY-STONE results for the site of Mylooi using parameters (E_N , E_T , and A_T) calibrated on the UAV DEM. The maximum translation kinetic energies are shown for (a) UAV DEM, (b) Greek Cadastral DEM, (c) ALOS AW3D30 DEM, (d) ASTER GDEM, and (e) SRTM30 DEM.

The comparison of the slope profile from the various DEMs reveals that finer resolutions depict a more detailed and precise topography. Figures 8 and 9, from the UAV DEM and Greek Cadastral DEM, respectively, demonstrate a more accurate slope decline compared to the broader and smoother profiles from coarser-resolution DEMs. The UAV DEM, with the finest resolution, shows a detailed descent pattern (Figure 8a), whereas the Greek Cadastral DEM, though slightly coarser (Figure 8b), still maintains a good level of detail. In contrast, DEMs such as the ALOS AW3D30, ASTER GDEM, and SRTM30 DEM (Figure 8c–e) offer progressively less detail as their resolution decreases, which simplifies the terrain's complexities. Additionally, the contour lines from the ASTER GDEM (Figure 7d) show a wider spacing compared to those from the ALOS AW3D30 (Figure 7c) and SRTM30 DEMs (Figure 7e). This broader spacing of contour lines and the less detailed slope profile could account for the notably lower values of maximum translational kinetic energy that were recorded by the ASTER GDEM (Figure 7d).

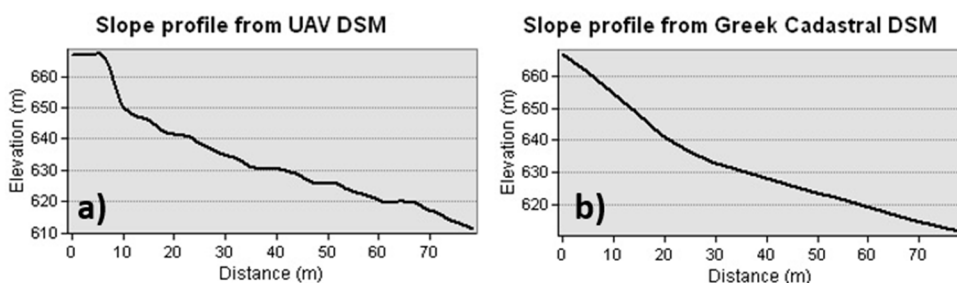


Figure 8. Cont.

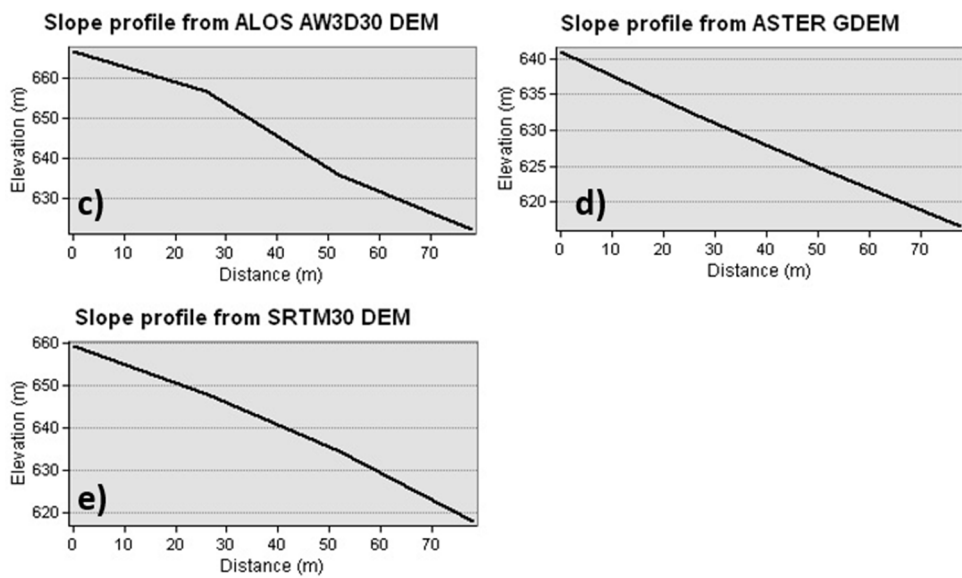


Figure 8. Slope profiles from (a) UAV DSE, (b) Greek Cadastral DEM, (c) ALOS AW3D30 DEM, (d) ASTER GDEM, and (e) SRTM30 DEM.

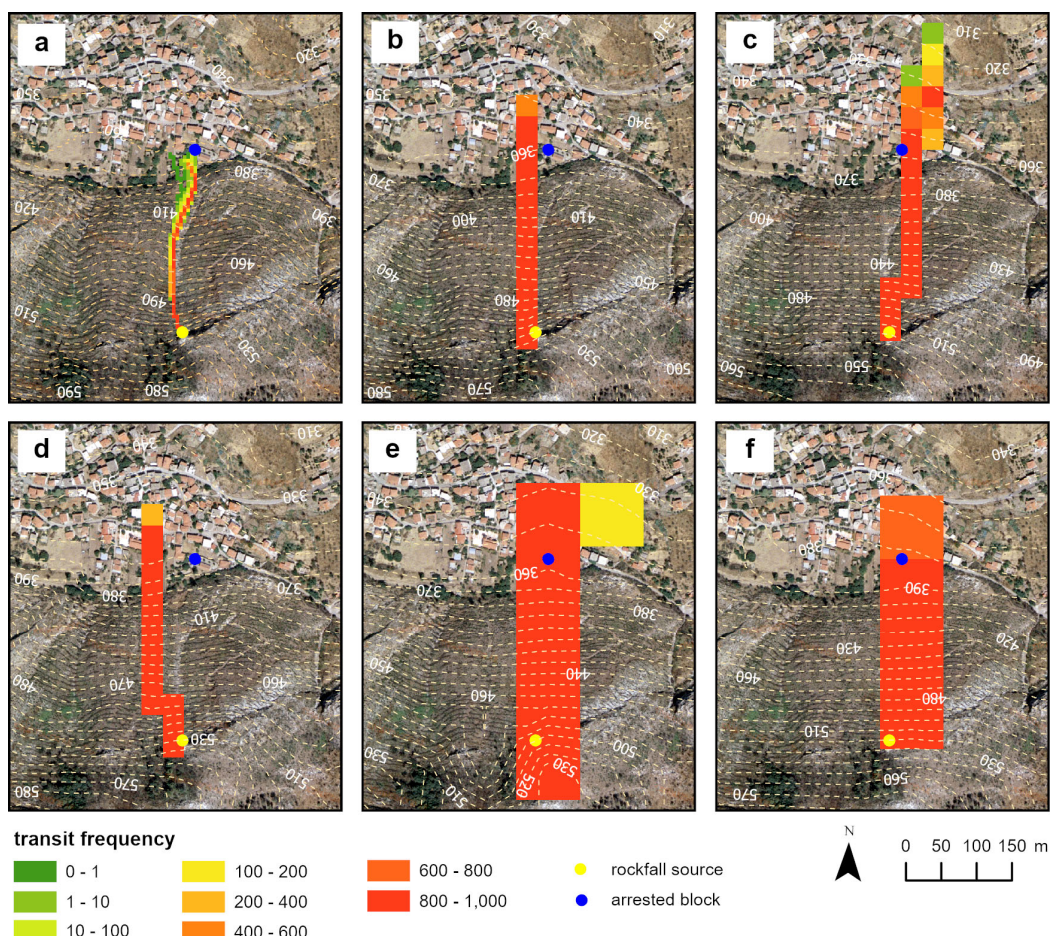


Figure 9. HY-STONE results, in terms of transit frequency for the site of Platiana. (a) Greek Cadastral DEM, (b) ALOS AW3D30 DEM, (c) ASTER GDEM, (d) SRTM30 DEM, (e) SRTM90 DEM, and (f) TanDEM_X.

4.1.2. Platiana Rockfall

For the Platiana rockfall analysis, six DEMs, including the Greek Cadastral DEM, ALOS AW3D30 DEM, ASTER GDEM, SRTM30 DEM, SRTM90 DEM, and TanDEM_X, were used, covering a resolution range from 5 m to 90 m. The coefficients of restitution E_N and E_T and the rolling friction coefficient A_T were back-calibrated on the higher-resolution DEM based on the rockfall event (Table 2). In this scenario, two masonry stone walls are located at the base of the slope and simulated with low values of E_N and E_T and high values of A_T , similar to buildings. Given that HY-STONE operates on a stochastic model, simulations were performed with 1000 rocks to provide a more accurate representation of the rockfall dynamics.

Table 2. Coefficients of restitution and rolling friction in Platiana rockfall, calibrated on the Greek Cadastral DEM.

Description	E_N	E_T	A_T
Houses	0.20	0.20	1.00
Road-asphalt	0.55	0.70	0.25
Debris well vegetated	0.35	0.60	0.42
Debris without vegetation	0.40	0.65	0.35
Stone wall	0.20	0.20	1.00

Figure 9a illustrates the transit frequency of the rocks using the Greek Cadastral DEM. High values are observed throughout the rockfall path, with a decrease in frequency from the midpoint to the endpoint of the rock trajectory. The transit frequency data extends almost up to the point where the rocks stop moving. More accurately, the rockfall trajectory ended just to the left of the actual endpoint.

All other considered DEMs simulated rock transits that extended beyond the actual rockfall path. The ALOS AW3D30 DEM exhibited a trajectory that passed from the left side of the real rock endpoint and captured high values from the rockfall source to the endpoint, with the values diminishing past the point where the rocks stopped (Figure 9b). The ASTER GDEM showed similar results but followed a distinct trajectory that crossed the rock stop point (Figure 9c). Meanwhile, the SRTM30 DEM also recorded high values at the rockfall source, which gradually decreased along a separate pathway, showing low values beyond the rock endpoint (Figure 9d). As is the case with the ALOS AW3D30 DEM, the SRTM30 DEM rockfall simulation also passed from the left side of the real endpoint.

The SRTM90 DEM and TanDEM_X, both with a 90 m spatial resolution, simulated the rock transit frequency in a less realistic manner (Figure 9e,f). Each recorded high values from the rockfall source to the endpoint and then displayed lower values past the endpoint. Specifically, the simulation using the SRTM90 DEM depicted a trajectory that extended beyond the actual endpoint, terminating on its right side. Meanwhile, the simulation with TanDEM_X also surpassed the real endpoint but continued along its initial trajectory.

The following data presents the maximum translational kinetic energies for the Platiana rockfall, expressed in kJ (Figure 10).

The outcomes based on the maximum translational kinetic energy from the Greek Cadastral are displayed in Figure 10a. The map, generated using HY-STONE within a GIS environment, shows high to very high kinetic energies near the rockfall source and in the central area, which then progressively decrease to very low levels towards the end of the slope. The maximum translational kinetic energy values range from 0 to 1500 kJ.

The computation of the maximum translational kinetic energy using the ALOS AW3D30 DEM is depicted in Figure 10b. This DEM outlined a single trajectory where kinetic energies near the rockfall source area are very low, ranging from 0 to 1 kJ, escalating to high energies between 100 to 1500 kJ in the middle of the path and tapering to medium energies from 0.2 to 100 kJ towards the end of the path. Conversely, the ASTER GDEM and SRTM30 DEM delineated multiple paths: low energies in the rockfall source area (0–1 kJ), high energies in the middle part (100–1500 kJ), and medium energies in the residential areas

(0.1–100 kJ), as shown in Figure 10c,d. All the DEMs with a 30 m spatial resolution thus calculated energies extending beyond the actual endpoint of the rockfall.

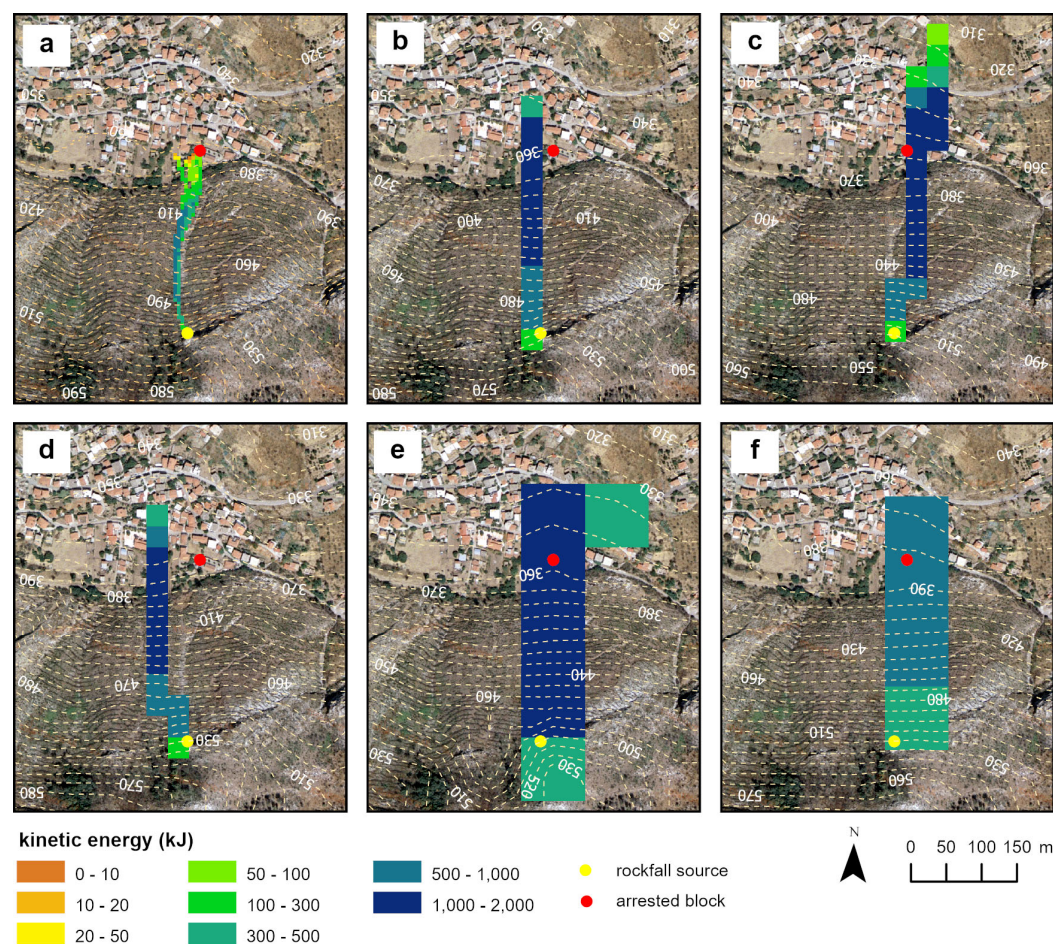


Figure 10. HY-STONE results in terms of the maximum translation kinetic energy for the site of Platiana. (a) Greek Cadastral DEM, (b) ALOS AW3D30 DEM, (c) ASTER GDEM, (d) SRTM30 DEM, (e) SRTM90 DEM, and (f) TanDEM_X.

Figure 10e illustrates the computation using the SRTM90 DEM, which generated two paths that were characterized by very high kinetic energies (500–1500 kJ) at the endpoint of the rockfall and low energies (0.2–1 kJ) near the source area. In contrast, the TanDEM_X mapped a single trajectory (Figure 10f) that displays a progression of medium, high, very high, back to medium, and then low energies, starting from the source area and extending beyond the actual endpoint of the rockfall. Both DEMs calculated kinetic energies that continued past the real endpoint of the rockfall.

The slope profiles (Figure 11) from the DEMs reveal differences in the elevation representation that correlate with the DEMs' spatial resolutions. The Greek Cadastral DEM (Figure 11a) provides a detailed topography due to its higher resolution, with an abrupt elevation drop, suggesting a potentially steeper terrain. In contrast, DEMs with coarser resolutions, such as the ALOS AW3D30 DEM (Figure 11b), ASTER GDEM (Figure 11c), SRTM30 DEM (Figure 11d), SRTM90 DEM (Figure 11e), and TanDEM_X (Figure 11f), show smoother elevation transitions, which might under-represent the actual terrain roughness. Also, the contour lines vary based on the spatial resolution of each DEM, as observed in Figure 10a–f. This variation influences the hillshade, which in turn affects the rockfall trajectories modeled by the HY-STONE software. Consequently, these differences in terrain representation explain the diversity of the rockfall simulations generated by the

software, concluding that the path of the rockfall trajectory in the Platiana site is an issue of the topography.

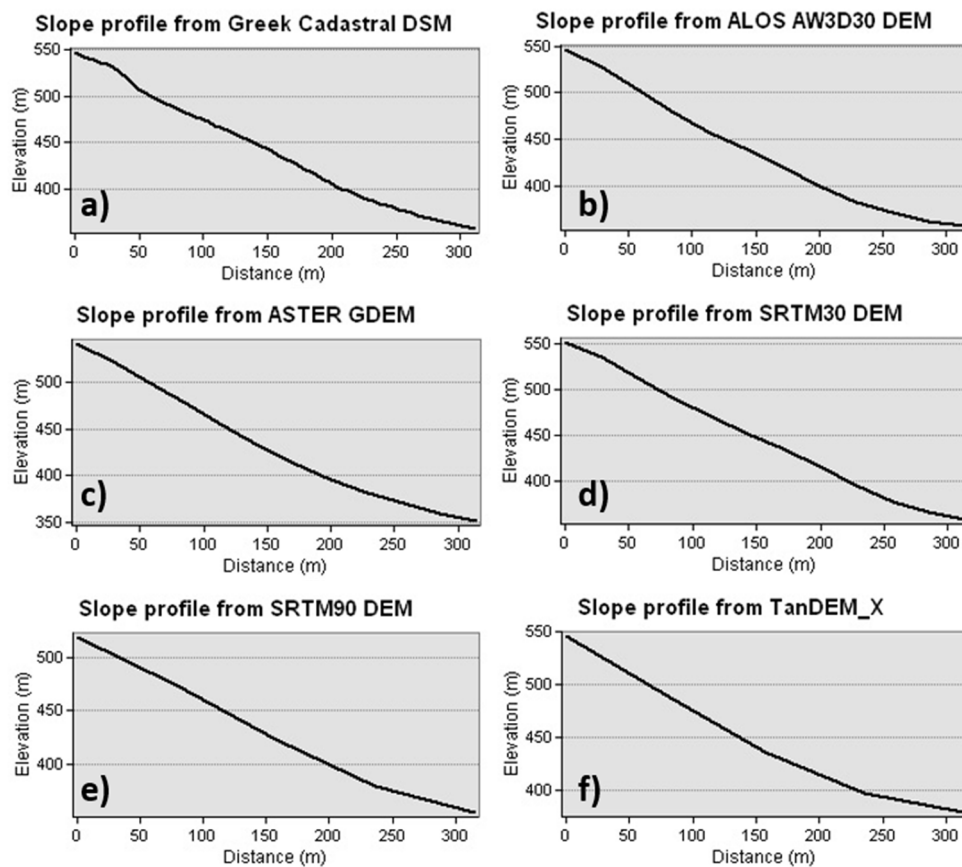


Figure 11. Slope profiles from (a) Greek Cadastral DEM, (b) ALOS AW3D30 DEM, (c) ASTER GDEM, (d) SRTM30 DEM, (e) SRTM90 DEM, and (f) TanDEM_X.

4.2. Results by Using Different Restitution Coefficients and Rolling Friction Coefficient

Considering the overestimation of the maximum runout distance projected by the simulations of both case studies with the low-resolution DEMs, a calibration of the normal (E_N) and tangential (E_T) coefficients of restitution, as well as the rolling friction coefficient (A_T) is required. In this section, the values of these coefficients are manually adjusted for each DEM scenario to obtain simulations that more closely resemble actual events. Specifically, to reduce the simulated runout distances, progressively lower restitution coefficients and higher friction coefficients are tested until the observation is matched. These adjustments compensate for different morphological roughness represented in each DEM.

4.2.1. Myloi Rockfall

After the coefficient adjustment procedure, it was determined that, for the Myloi case, only the Greek Cadastral DEM yielded reliable results, as the other DEMs (ALOS AW3D30 DEM, ASTER GDEM, SRTM30 DEM, SRTM90 DEM, and TanDEM_X) proved unsuitable for small-scale events like the Myloi rockfall, leading to unrealistic outputs. Regarding the UAV DEM, no new trials were conducted as the results with the initial coefficient values already align with the in situ observations. The forthcoming results showcase the transit frequency and maximum translational kinetic energy from the Greek Cadastral DEM, obtained with the revised coefficients shown in Table 3.

Table 3. Optimal coefficients for the Myloi rockfall using the Greek Cadastral DEM.

Description	E_N	E_T	A_T
Houses	0.20	0.20	1.00
Road-asphalt	0.35	0.55	0.50
Debris well vegetated	0.20	0.45	0.80
Debris without vegetation	0.25	0.50	0.70

The results from the Greek Cadastral DEM reveal that the transit frequency values were high, nearing 1000, in the rockfall source area and along the main rockfall path (Figure 12a). In terms of the maximum translational kinetic energy, the HY-STONE calculations showed energy levels ranging from 0 to 500 kJ. The rockfall source area and the endpoint recorded minimal energies, whereas the main body exhibited significantly higher energies, up to 500 kJ (Figure 12b). This simulation using the Greek Cadastral DEM accurately reflects the actual rockfall event.

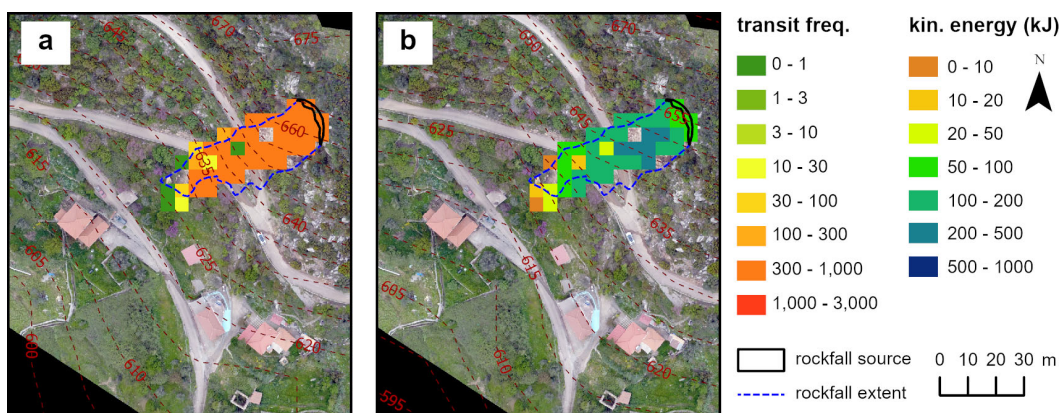


Figure 12. HY-STONE results by using the Greek Cadastral DEM with the optimal coefficients shown in Table 3 for the site of Myloi: (a) the transit frequency and (b) the maximum translation kinetic energy.

Figures 6b and 12a from the HY-STONE simulations illustrate the effect of coefficient customization on rockfall modeling accuracy for the Myloi site by using the Greek Cadastral DEM at a 5 m resolution. In Figure 12a, where the values of the coefficients were fine-adjusted to match the in situ observations, the depicted rockfall trajectories accurately terminate at the exact rock endpoints that were observed on-site, demonstrating a precise localization of rockfall impact. In contrast, Figure 6b uses standard empirically derived coefficients, resulting in trajectories that extend beyond the actual observed endpoints, suggesting an overestimation of the impact area. This comparison highlights the importance of adjusting the simulation parameters to specific site conditions to ensure the accuracy and reliability of rockfall risk assessments. Furthermore, Figures 7b and 12b illustrate the HY-STONE results for the maximum translation kinetic energy, also at the Myloi site, using the Greek Cadastral DEM at a 5 m resolution. As can be seen in Figure 12b, utilizing the adjusted coefficients for a closer match to the in situ observations shows a precise distribution of kinetic energy with high values concentrated near the rockfall source, thus closely reflecting the actual rockfall paths. In contrast, Figure 7b employs empirically derived coefficients, resulting in a more dispersed and extended kinetic energy distribution across the area.

4.2.2. Platiana Rockfall

For the Platiana rockfall, the coefficients E_N , E_T , and A_T have been adjusted for each DEM scenario, except for the Greek Cadastral DEM, which was already calibrated in the previous section against the in situ observations. Presented next are the outcomes for the

transit frequency and maximum translational kinetic energy from the simulations using the ALOS AW3D30 DEM, ASTER GDEM, SRTM30 DEM, SRTM90 DEM, and TanDEM_X using the optimal restitution and rolling friction coefficients for each scenario.

Table 4 and Figure 13 showcase the optimal coefficients and simulation results in terms of the transit frequency and kinetic energies for the ALOS AW3D30 DEM.

Table 4. Optimal coefficients for the Platiana rockfall using the ALOS AW3D30 DEM.

Description	E_N	E_T	A_T
Houses	0.20	0.20	1.00
Road-asphalt	0.45	0.60	0.40
Debris well vegetated	0.25	0.45	0.64
Debris without vegetation	0.30	0.55	0.50
Stone wall	0.20	0.20	1.00

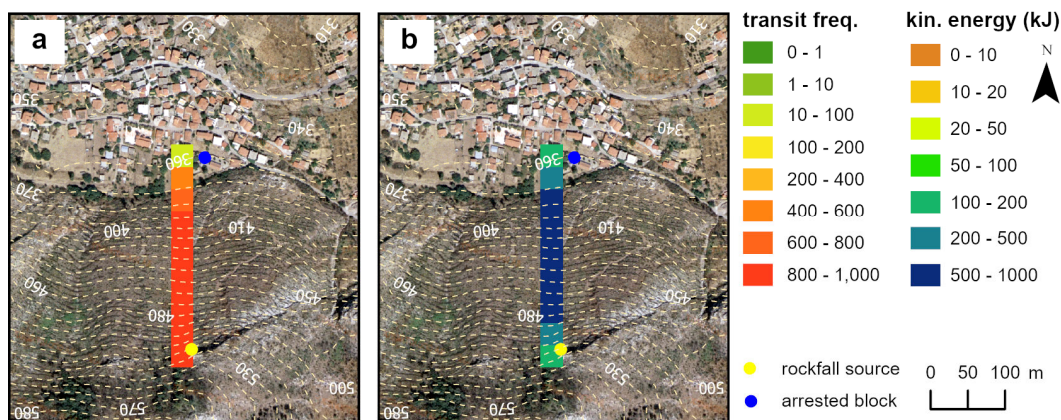


Figure 13. HY-STONE results by using the ALOS AW3D30 DEM with optimal coefficients shown in Table 4 for the site of Platiana: (a) the transit frequency and (b) the maximum translation kinetic energy.

According to Figure 13a, the ALOS AW3D30 DEM exhibited a single corridor of trajectories that pass on the left side of the real rock endpoint and show only low transit frequencies close to the endpoint. The computation of maximum translational kinetic energy displayed a range of values, beginning with low energies (50–100 kJ), escalating to very high energies (500–1000 kJ), and finally ending again with low energies (50–100 kJ) before reaching the endpoint (Figure 13b).

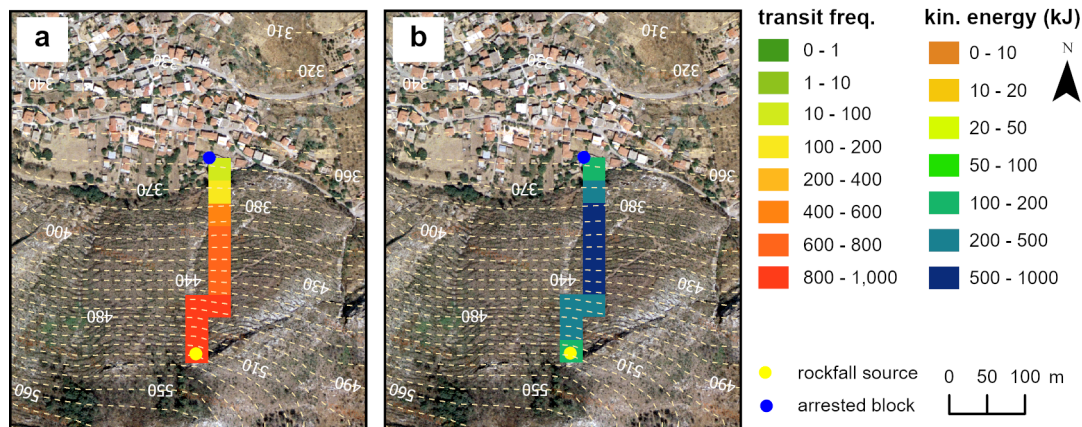
The comparison between Figures 13a and 9b highlights the differences in the transit frequency before and after the parameter adjustment. While Figure 13a depicts a very concentrated narrow path, suggestive of a well-defined rockfall trajectory, Figure 9b shows a more dispersed and broad frequency distribution that extends beyond the actual observed endpoints, implying either different simulation settings or more complex terrain interactions. Similarly, Figures 10b and 13b contrast in their portrayal of kinetic energy; Figure 13b presents a linear decrease in energy from the source along a controlled path, whereas Figure 10b depicts a diffuse energy pattern with values further from the rock endpoint.

Table 5 and Figure 14 showcase the optimal coefficients and simulation results in terms of the transit frequency and kinetic energies for the ALOS AW3D30 DEM.

Regarding the transit frequency maps, the ASTER GDEM documented (Figure 14a) high to low transit frequencies during the rock path crossing the rock stop point.

Table 5. Optimal coefficients for the Platiana rockfall using the ASTER GDEM.

Description	E_N	E_T	A_T
Houses	0.20	0.20	1.00
Road-asphalt	0.45	0.58	0.38
Debris well vegetated	0.22	0.42	0.69
Debris without vegetation	0.27	0.52	0.48
Stone wall	0.20	0.20	1.00

**Figure 14.** HY-STONE results by using the ASTER GDEM with the optimal coefficients shown in Table 5 for the site of Platiana: (a) the transit frequency and (b) the maximum translation kinetic energy.

Concerning the kinetic energy calculations, the ASTER GDEM develops similarly to the ALOS AW3D30 DEM simulation, starting with low values, followed by an increase until the final part of the trajectories where the blocks stopped.

Figure 14a presents a single concentrated transit frequency along a narrow path, reflecting a precise and realistic depiction of rockfall trajectory. In contrast, Figure 9c results in a broader and less defined distribution of transit frequencies, indicating multiple potential trajectories and a potential overestimation of the impact area. According to the kinetic energies, Figure 10c shows a detailed gradient of kinetic energy with multiple zones ranging from low- to high-energy values, reflecting a nuanced understanding of energy dissipation along the trajectory. This gradient indicates a more refined simulation where kinetic energy decreases progressively from the source, offering a detailed perspective on energy distribution during rockfall. On the other hand, Figure 14b exhibits a more simplified energy distribution, primarily concentrating high kinetic energy near the rockfall source with a sharp drop to lower values, suggesting a less complex interaction with the terrain.

Table 6 and Figure 15 showcase the optimal coefficients and simulation results in terms of the transit frequency and kinetic energies for the SRTM30 DEM.

Table 6. Optimal coefficients for the Platiana rockfall using the SRTM30 DEM.

Description	E_N	E_T	A_T
Houses	0.20	0.20	1.00
Road-asphalt	0.45	0.60	0.40
Debris well vegetated	0.25	0.45	0.64
Debris without vegetation	0.30	0.55	0.50
Stone wall	0.20	0.20	1.00

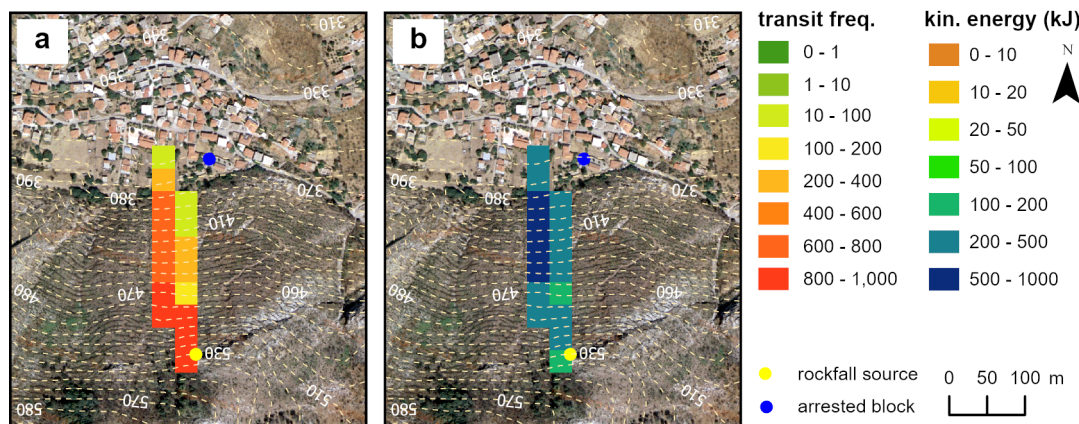


Figure 15. HY-STONE results by using the SRTM30 DEM with the optimal coefficients shown in Table 6 for the site of Platiana: (a) the transit frequency and (b) the maximum translation kinetic energy.

The SRTM30 DEM displayed medium transit frequencies over an extended section of the rock path, high frequencies in the source area, and no recorded values at the rock endpoint (Figure 15c). The kinetic energy results delineated two rock paths: the left, with energy levels up to 500–1000 kJ, and the right, with lower values around 200 kJ (Figure 15d).

Figure 9d, Figure 10d, and Figure 15a,b present the rockfall simulation results for the transit frequency and kinetic energies, correspondingly, using the SRTM30 DEM. Figure 15a,b uses the adjusted coefficients, while Figures 9d and 10d use coefficients on the highest resolution DEM. Figure 15a shows a more diverse color spectrum, indicating a dynamic interaction with a varied terrain that ends at the left side of the rock endpoint, while Figure 9d presents a more uniform and concentrated frequency, suggesting simpler terrain interactions or model settings that end after the rock endpoint. Figure 10d displays a linear distribution of kinetic energy with clear high-energy zones concentrated near the rockfall source, suggesting a direct rockfall trajectory. In contrast, Figure 15b shows a more uniform distribution, with fewer fluctuations in energy levels along the trajectory, indicating a potential oversimplification of the terrain's impact on energy dissipation.

Table 7 and Figure 16 showcase the optimal coefficients and simulation results in terms of the transit frequency and kinetic energies for the SRTM90 DEM.

Table 7. Optimal coefficients for the Platiana rockfall using the SRTM90 DEM.

Description	E_N	E_T	A_T
Houses	0.20	0.20	1.00
Road-asphalt	0.42	0.55	0.45
Debris well vegetated	0.22	0.40	0.70
Debris without vegetation	0.28	0.50	0.55
Stone wall	0.20	0.20	1.00

The SRTM90 DEM shows a constant decrease in the transit frequencies along the slope (Figure 16a), resembling the results of the ASTER GDEM and ALOS AW3D30 DEM. Regarding the kinetic energy (Figure 16b), the SRTM90 DEM exhibited initial lower energies of 200–500 kJ at the source area, increasing to 500–1000 kJ along the slope, without any decrease in energy before the rock stop point (Figure 16b).

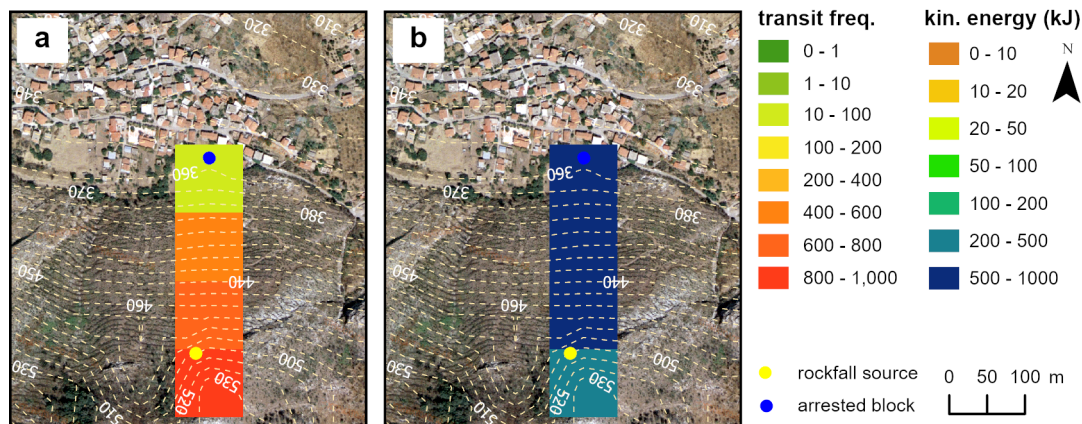


Figure 16. HY-STONE results by using the SRTM90 DEM with the optimal coefficients shown in Table 7 for the site of Platiana: (a) the transit frequency and (b) the maximum translation kinetic energy.

The transit frequency results shown in Figures 9e and 16a demonstrate a vertical layout with varying degrees of distribution; Figure 9e shows a poor gradation of the frequency zones along the slope continuing after the rock endpoint, whereas Figure 16a presents a more streamlined frequency layout ending at the rock endpoint. Similarly, the kinetic energy results in Figures 10e and 16b display linear energy distributions along the rockfall path. Figure 10e shows a complex pattern of low- and high-energy zones near the rockfall source and at the endpoint. On the other hand, Figure 16b portrays a simpler and more uniform distribution of kinetic energy, highlighting the role of the model's parameters in shaping the energy dissipation outcomes.

Table 8 and Figure 17 showcase the optimal coefficients and simulation results in terms of the transit frequency and kinetic energies for the TanDEM_X.

Table 8. Optimal coefficients for the Platiana rockfall using the TanDEM_X.

Description	E_N	E_T	A_T
Houses	0.20	0.20	1.00
Road-asphalt	0.35	0.52	0.48
Debris well vegetated	0.20	0.38	0.72
Debris without vegetation	0.25	0.47	0.58
Stone wall	0.20	0.20	1.00

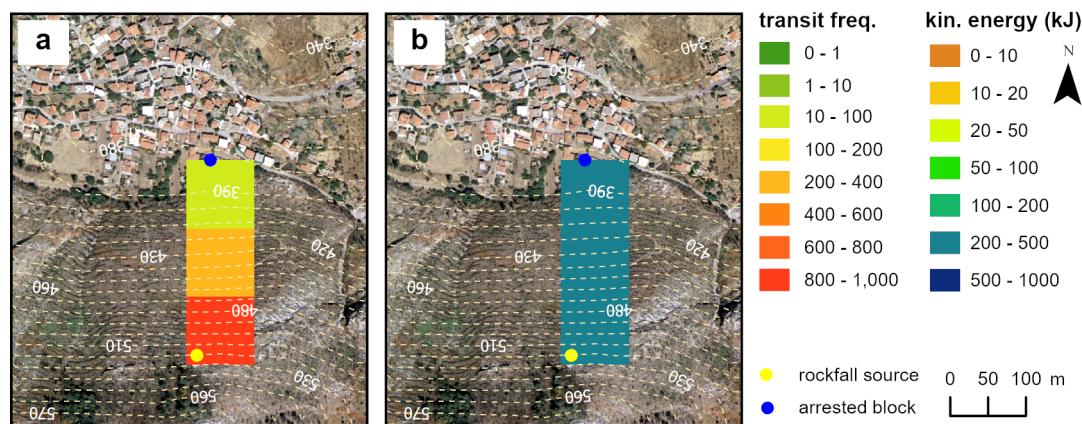


Figure 17. HY-STONE results by using the TanDEM_X with the optimal coefficients shown in Table 8 for the site of Platiana: (a) the transit frequency and (b) the maximum translation kinetic energy.

According to the TanDEM_X rockfall simulation map, the transit frequency for the Platiana rockfall is high in the source area and low at the endpoint of the rockfall (Figure 17a). The maximum translational kinetic energies show little variation along the slope, ranging in the 200–500 kJ class (Figure 17b).

The comparison between Figures 17a and 9f concluded that the simulation with the parameters optimized on the TanDEM_X presents a simplified and very linear representation of the transit frequency ending at the rock endpoint, which strictly follows a vertical pattern, indicating a highly targeted and specific rockfall path. Meanwhile, Figure 9f displays a more complex distribution with a smaller spectrum of transit frequencies, suggesting more variability in rockfall behavior. Last but not least, the compared Figures 17b and 10f sum up that both figures show a constant vertical distribution of kinetic energy values, but Figure 17b depicts a less spread-out energy distribution with a more realistic ending point.

To explore how the spatial resolution of the DEMs influences the normal (E_N) and tangential (E_T) restitution coefficients and the rolling friction coefficient (A_T), a plot reporting the differences in the coefficients for the most representative land cover class (debris without vegetation) is shown for the Platiana case (Figure 18). This plot clearly shows that the optimal normal (E_N) and tangential (E_T) coefficients decrease with increasing spatial resolution, whereas the rolling friction coefficient (A_T) increases with a higher spatial resolution.

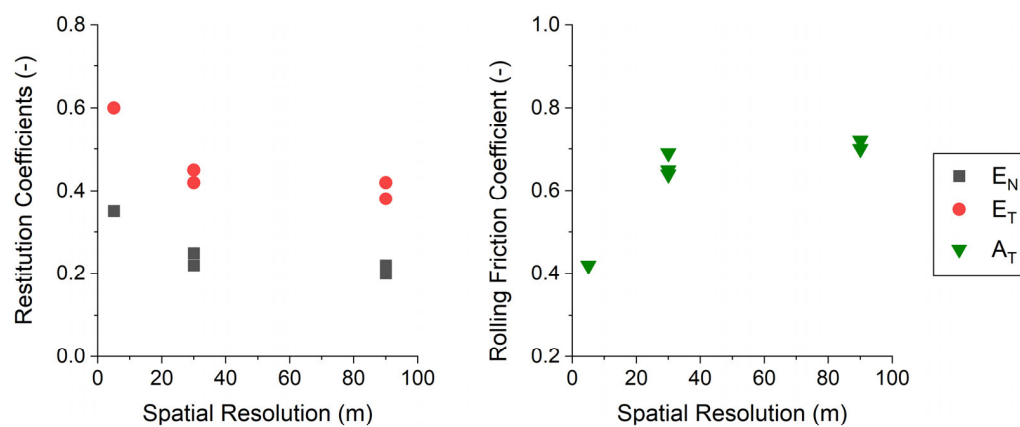


Figure 18. The effect of spatial resolution in the normal (E_N) and tangential (E_T) restitutions and the rolling friction (A_T) coefficients. For 30 m and 90 m, three and two DEMS are available, respectively.

The graph shows a roughly logarithmic relationship between the spatial resolution of DEMs and the optimal rockfall simulation coefficients. As the pixel size increases, indicative of coarser spatial resolution, the rolling friction coefficient (A_T) exhibits an increasing trend. This suggests that larger pixel sizes, which represent less detailed terrain data, demand high values of rolling friction coefficient to halt rocks more rapidly on the slope.

In contrast, the restitution coefficients, E_N and E_T , show a decreasing trend with increasing pixel size. This pattern indicates that, in simulations, rocks lose more energy upon impact with coarser-resolution DEMs, resulting in shorter bounces and less travel distance, which is characteristic of more inelastic collisions.

The correlation depicted here highlights the significance of selecting DEMs with appropriate pixel sizes for rockfall modeling to ensure that the physical behavior of rockfalls is realistically replicated in the simulation outcomes. The variability of the coefficients for a certain resolution is due to slight differences in the morphological description of the different DEMs. Future research will expand the dataset to validate these findings further. However, the observed trend provides valuable insights into the behavior of each coefficient in relation to each spatial resolution.

5. Discussion

The use of HY-STONE in analyzing rockfall simulations across different DEMs has highlighted the pivotal role of spatial resolution in the accuracy of rockfall modeling outcomes. The detailed analyses from the rockfall events at Myloi and Platiana, utilizing DEMs with a broad range of resolutions, confirm that higher-resolution DEMs, such as the UAV DEM and Greek Cadastral DEM, produce more accurate simulations of rockfall trajectories, aligning with our field observations. This finding is in line with previous studies suggesting that finer resolutions enhance the simulation's precision due to their ability to capture critical topographical details [34,36,41]. Remote sensing techniques, as used in this research, offer significant advantages by minimizing the data collection time and enabling access to otherwise inaccessible areas, thus enhancing the efficiency of rockfall hazard assessments [11,29,42]. This study further highlights the variations in performance among high-resolution DEMs, highlighting the importance of careful DEM selection based on the specific characteristics of a rockfall area and the methodologies behind data collection and processing [36].

This study extends the previous findings by not only confirming the influence of spatial resolution on simulation accuracy but also exploring how HY-STONE's capabilities can be optimized through strategic DEM selection. Large differences in the results can be observed by using the same parameter sets with different DEMs, with a longer runout simulated for coarser DEMs and a shorter runout with more resolute DEMs [36]. This effect can be attributed to the different ruggedness of DEMs as a function of the cell size [30]. For instance, the discrepancies in simulation outcomes among various high-resolution DEMs prompt a recommendation for future research to develop more sophisticated algorithms within HY-STONE. While the influence of DEM resolution is clear, DEMs created using distinct algorithms require unique parameter sets, even when sharing the same cell size [36]. These algorithms would compensate for the limitations of lower-resolution DEMs, especially in economically constrained settings where high-resolution DEMs are not feasible [32].

Previous studies using HY-STONE software for rockfall simulations also emphasize the critical role of the selected DEM and the calibration of its three coefficients concluding to similar results. It has been noted that an improved DEM accuracy correlates directly with higher precision in the HY-STONE simulation results, particularly with a target grid resolution of one meter by one meter or less in the volume scenarios from local-scale rockfalls [37,38,43,44] and a grid resolution of five meters by five meters for larger-scale rockfalls.

In this paper, it has been highlighted that the proper calibration of restitution and friction coefficients can compensate for the effects of different morphological roughness, represented in each DEM, by reaching satisfactory results, even with coarser-resolution DEMs. Different degrees of accuracy compared to the high spatial resolution simulations are achieved in terms of the transit frequencies and kinetic energies. Furthermore, for small-scale events, low-resolution DEMs are unsuitable for reliable predictions, such as the case of the Myloi rockfall. Another limitation of DEMs with coarser resolutions is how the rockfall source area is located inside large pixels, which could lead to potential misfits of the initial trajectory, leading to very large errors in the final outcome. This limitation cannot be overcome by parameter optimization; however, it is a potential improvement in the development of the HY-STONE software.

Additionally, the role of vegetation cover in influencing rockfall trajectories has been reaffirmed [33,45,46]. Studies have shown that vegetation can significantly impact the path and energy of falling rocks, emphasizing the need for HY-STONE to incorporate the vegetation parameters effectively [33]. Future studies should also investigate the integration of multiple DEMs to refine the predictive capabilities and adapt to the constraints of resource-limited settings. Ultimately, this discussion emphasizes the necessity of using high-resolution DEMs for detailed and accurate rockfall modeling, particularly when employing HY-STONE software. The continuous refinement of DEMs and the integration

of new data sources, such as UAV photogrammetry, are crucial for advancing rockfall simulation techniques and improving the reliability of rockfall hazard assessments.

This research provides a substantial contribution to the geoscience field, particularly in rockfall hazard management and mitigation. By evaluating the impact of a DEM's spatial resolution on 3D rockfall simulations within a GIS environment, this study offers key insights into the optimization of rockfall prediction models. It shows how different DEM resolutions affect the accuracy of rockfall trajectory simulations, which is crucial for effective hazard assessments and planning in vulnerable areas. This advancement allows for better-informed decision-making regarding land use and civil protection measures in areas prone to rockfalls. Moreover, the study's methodological approach, utilizing the HY-STONE software for detailed multiscale analyses, sets a new benchmark in the field. It paves the way for further research on the integration of various DEMs and modeling techniques to refine rockfall hazard predictions. Ultimately, this research not only progresses our scientific understanding but also contributes to improving public safety and infrastructure protection in rockfall-prone regions.

6. Conclusions

This research exemplifies the application of HY-STONE in modeling rockfalls of varying scales. The software performs effectively for both small-scale events, as shown in the Mylooi settlement, and larger-scale occurrences, such as the Platiana rockfall, by appropriately selecting and adjusting DEMs and simulation parameters. The variability in results between different DEMs emphasizes the importance of selecting the correct spatial resolution for a given rockfall scenario. The spatial resolution directly influences the ability of the HY-STONE software to produce simulations that closely resemble the physical behavior observed in real-world events.

The results highlight the critical role of spatial resolution in rockfall modeling, with finer-resolution DEMs providing the superior detail necessary for precise modeling outcomes. The analysis indicates that high-resolution DEMs not only provide a detailed terrain representation crucial for identifying rockfall sources but also enhance the accuracy of kinetic energy distribution in the simulations. In this study, the comparative analysis of a multitude of freely available DEMs within HY-STONE reveals the significance of choosing the right model for a given scenario, with higher resolutions preferred for detailed local-scale analyses. This study also highlights the importance of empirical knowledge and calibration against field data in setting the restitution and rolling friction coefficients, which significantly influence the behavior of simulated rockfalls.

More specifically, the results show that:

1. By maintaining constant values for the restitution and rolling friction coefficients (determined empirically) for the Mylooi rockfall, the UAV DEM with a spatial resolution of 0.05 m led to the most reliable simulation via HY-STONE, as the transit frequency stopped precisely where the rocks did, thus matching the *in situ* observations.
2. In the case of the Platiana rockfall, keeping the aforementioned empirically defined coefficients constant, the Greek Cadastral DEM with a 5 m spatial resolution yielded results that most closely resembled the actual rockfall.
3. By altering the E_N , E_T , and A_T parameters, for the Mylooi rockfall, only the Greek Cadastral DEM provided a reliable representation. DEMs with larger spatial resolutions did not lead to an accurate rockfall simulation due to the small scale of the event and the DEMs' pixel size being too large to capture detailed results.
4. In contrast, for the Platiana rockfall, which is a larger-scale event, changing the E_N , E_T , and A_T parameters—specifically, decreasing E_N and E_T and increasing A_T as the spatial resolution increased—resulted in simulations through HY-STONE that increasingly resembled the actual rockfall event.
5. In all instances, the topography depicted by the DEMs with a spatial resolution exceeding 30 m showed a minimal variation in the HY-STONE rockfall simulations.

To sum up, the most accurate results are those obtained by keeping the restitution and rolling friction coefficients constant, as they have been established based on empirical experience. Regarding the spatial resolution of the DEMs, the finer the pixel size, the closer to reality the simulation will be. This suggests that high-resolution DEMs should be prioritized when available and are applicable to rockfall studies.

Author Contributions: Conceptualization, K.G.N. and M.P.K.; methodology, M.P.K. and P.F.; software, P.F., A.P. and M.P.K.; validation, P.F. and A.P.; investigation, K.G.N. and M.P.K.; data curation, K.G.N. and M.P.K.; writing—original draft preparation, M.P.K., P.F. and A.P. writing—review and editing, K.G.N. and P.F.; supervision, K.G.N. All authors have read and agreed to the published version of the manuscript.

Funding: This research received no external funding.

Data Availability Statement: The data are part of the 1st author PhD thesis, therefore there are restrictions to share.

Conflicts of Interest: The authors declare no conflict of interest.

References

1. Fell, R.; Corominas, J.; Bonnard, C.; Cascini, L.; Leroi, E.; Savage, W.Z. Guidelines for landslide susceptibility, hazard and risk zoning for land use planning. *Eng. Geol.* **2008**, *102*, 85–98. [[CrossRef](#)]
2. Farvacque, M.; Eckert, N.; Candia, G.; Bourrier, F.; Corona, C.; Toe, D. Holistic rockfall risk assessment in high mountain areas affected by seismic activity: Application to the Uspallata valley, Central Andes, Chile. *Risk Anal.* **2024**, *44*, 1021–1045. [[CrossRef](#)]
3. Van Veen, M.; Hutchinson, D.J.; Bonneau, D.A.; Sala, Z.; Ondercin, M.; Lato, M. Combining temporal 3-D remote sensing data with spatial rockfall simulations for improved understanding of hazardous slopes within rail corridors. *Nat. Hazards Earth Syst. Sci.* **2018**, *18*, 2295–2308. [[CrossRef](#)]
4. Yomralioğlu, T. *Geographic Information Systems: Basic Concepts and Applications*; Akademi Publishing House: İstanbul, Turkeyie, 2009; p. 480. ISBN 975-97369-0-X.
5. Çellek, S. Effect of the Slope Angle and Its Classification on Landslide. *Nat. Hazards Earth Syst. Sci.* **2020**, *in press*. [[CrossRef](#)]
6. Keijsers, J.G.S.; Schoorl, J.M.; Chang, K.-T.; Chiang, S.-H.; Claessens, L.; Veldkamp, A. Calibration and resolution effects on model performance for predicting shallow landslide locations in Taiwan. *Geomorphology* **2011**, *133*, 168–177. [[CrossRef](#)]
7. Pradhan, B.; Sameen, M.I. Effects of the Spatial Resolution of Digital Elevation Models and Their Products on Landslide Susceptibility Mapping. In *Laser Scanning Applications in Landslide Assessment*; Springer: Berlin/Heidelberg, Germany, 2017; pp. 133–150.
8. Acosta, E.; Agliardi, F.; Crosta, G.B.; Ríos Aragues, S. Regional Rockfall Hazard Assessment in the Benasque Valley (Central Pyrenees) Using a 3D Numerical Approach. In Proceedings of the 4th EGS Plinius Conference—Mediterranean Storms, Mallorca, Spain, 2–4 October 2002; pp. 555–563.
9. Baillifard, F.; Jaboyedoff, M.; Sartori, M. Rockfall hazard mapping along a mountainous road in Switzerland using a GIS-based parameter rating approach. *Nat. Hazards Earth Syst. Sci.* **2003**, *3*, 435–442. [[CrossRef](#)]
10. Marquinez, J.; Menéndez Duarte, R.; Farias, P.; Jiménez Sánchez, M. Predictive GIS-Based Model of Rockfall Activity in Mountain Cliffs. *Nat. Hazards* **2003**, *30*, 341–360. [[CrossRef](#)]
11. Jaboyedoff, M.; Baillifard, F.; Philipposian, F.; Rouiller, J.-D. Assessing fracture occurrence using “weighted fracturing density”: A step towards estimating rock instability hazard. *Nat. Hazards Earth Syst. Sci.* **2004**, *4*, 83–93. [[CrossRef](#)]
12. Derron, M.-H.; Jaboyedoff, M.; Blikra, L.H. Preliminary assessment of rockslide and rockfall hazards using a DEM (Oppstadhornet, Norway). *Nat. Hazards Earth Syst. Sci.* **2005**, *5*, 285–292. [[CrossRef](#)]
13. Lan, H.; Derek Martin, C.; Lim, C.H. RockFall analyst: A GIS extension for three-dimensional and spatially distributed rockfall hazard modeling. *Comput. Geosci.* **2007**, *33*, 262–279. [[CrossRef](#)]
14. Loyer, A.; Jaboyedoff, M.; Pedrazzini, A. Identification of potential rockfall source areas at a regional scale using a DEM-based geomorphometric analysis. *Nat. Hazards Earth Syst. Sci.* **2009**, *9*, 1643–1653. [[CrossRef](#)]
15. Ravanel, L.; Allignol, F.; Deline, P.; Gruber, S.; Ravello, M. Rock falls in the Mont Blanc Massif in 2007 and 2008. *Landslides* **2010**, *7*, 493–501. [[CrossRef](#)]
16. Zieher, T.; Formanek, T.; Bremer, M.; Meissl, G.; Rutzinger, M. Digital Terrain Model Resolution and its Influence on Estimating the Extent of Rockfall Areas. *Trans. GIS* **2012**, *16*, 691–699. [[CrossRef](#)]
17. Palma, B.; Parise, M.; Reichenbach, P.; Guzzetti, F. Rockfall hazard assessment along a road in the Sorrento Peninsula, Campania, southern Italy. *Nat. Hazards* **2011**, *61*, 187–201. [[CrossRef](#)]
18. Corona, C.; Trappmann, D.; Stoffel, M. Parameterization of rockfall source areas and magnitudes with ecological recorders: When disturbances in trees serve the calibration and validation of simulation runs. *Geomorphology* **2013**, *202*, 33–42. [[CrossRef](#)]

19. Nikolakopoulos, K.; Depountis, N.; Vagenas, N.; Kavoura, K.; Vlaxaki, E.; Kelasidis, G.; Sabatakakis, N. Rockfall Risk Evaluation Using Geotechnical Survey, Remote Sensing Data, and GIS: A Case Study from Western Greece. In Proceedings of the Third International Conference on Remote Sensing and Geoinformation of the Environment (RSCy2015), Paphos, Cyprus, 19 June 2015.
20. Volkwein, A.; Schellenberg, K.; Labiouse, V.; Agliardi, F.; Berger, F.; Bourrier, F.; Dorren, L.K.A.; Gerber, W.; Jaboyedoff, M. Rockfall characterisation and structural protection—A review. *Nat. Hazards Earth Syst. Sci.* **2011**, *11*, 2617–2651. [\[CrossRef\]](#)
21. Stevens, W.D. RocFall, a Tool for Probabilistic Analysis, Design of Remedial Measures and Prediction of Rockfalls. Ph.D. Thesis, University of Toronto, Toronto, ON, Canada, 1998.
22. Rocscience. RocFall software—For risk analysis of falling rocks on steep slopes. In *Rocscience User's Guide*; Rocscience: Toronto, ON, Canada, 2002.
23. Hind, H. Comparison of 3D and 2D Rockfall Models: Considering Terrain Model Quality Effect on Respective Model Performances. Master's Thesis, UiT the Arctic University of Norway, Tromsø, Norway, 2018.
24. Kakavas, M.; Nikolakopoulos, K. Rock-fall simulation and validation with in situ data: The case of Moira settlement in Western Greece. In *Earth Resources and Environmental Remote Sensing/GIS Applications XII*; SPIE: Bellingham, Washington, USA, 2021; Volume 11863.
25. Abellán, A.; Vilaplana, J.M.; Martínez, J. Application of a long-range Terrestrial Laser Scanner to a detailed rockfall study at Vall de Núria (Eastern Pyrenees, Spain). *Eng. Geol.* **2006**, *88*, 136–148. [\[CrossRef\]](#)
26. Žabota, B.; Repe, B.; Kobal, M. Influence of digital elevation model resolution on rockfall modelling. *Geomorphology* **2018**, *328*, 183–195. [\[CrossRef\]](#)
27. Guzzetti, F.; Crosta, G.B.; Detti, R.; Agliardi, F. STONE: A computer program for the three-dimensional simulation of rockfalls. *Comput. Geosci.* **2002**, *28*, 1081–1095. [\[CrossRef\]](#)
28. Crosta, G.B.; Agliardi, F. A methodology for physically based rockfall hazard assessment. *Nat. Hazards Earth Syst. Sci.* **2003**, *3*, 407–422. [\[CrossRef\]](#)
29. Kakavas, M.; Nikolakopoulos, K. Digital Elevation Models of Rockfalls and Landslides: A Review and Meta-Analysis. *Geosciences* **2021**, *11*, 256. [\[CrossRef\]](#)
30. Crosta, G.B.; Agliardi, F. Parametric evaluation of 3D dispersion of rockfall trajectories. *Nat. Hazards Earth Syst. Sci.* **2004**, *4*, 583–598. [\[CrossRef\]](#)
31. Bühler, Y.; Christen, M.; Glover, J.; Bartelt, P. Significance of Digital Elevation Model Resolution for Numerical Rockfall Simulations. In Proceedings of the 3rd International Symposium Rock Slope Stability C2ROP, Lyon, France, 15–17 November 2016; pp. 15–17.
32. Frattini, P.; Crosta, G.; Carrara, A.; Agliardi, F. Assessment of rockfall susceptibility by integrating statistical and physically-based approaches. *Geomorphology* **2008**, *94*, 419–437. [\[CrossRef\]](#)
33. Agliardi, F.; Crosta, G.B.; Frattini, P. Integrating rockfall risk assessment and countermeasure design by 3D modelling techniques. *Nat. Hazards Earth Syst. Sci.* **2009**, *9*, 1059–1073. [\[CrossRef\]](#)
34. Agliardi, F.; Crosta, G.B. High resolution three-dimensional numerical modelling of rockfalls. *Int. J. Rock Mech. Min. Sci.* **2003**, *40*, 455–471. [\[CrossRef\]](#)
35. Themistocleous, K.; Danezis, C. Monitoring cultural heritage sites affected by geo-hazards using in situ and SAR data: The Choirokoitia case study. In *Remote Sensing for Archaeology and Cultural Landscapes: Best Practices and Perspectives Across Europe and the Middle East*; Springer: Berlin/Heidelberg, Germany, 2020; pp. 285–308.
36. Frattini, P.; Crosta, G.B.; Agliardi, F.; Imposimato, S. Challenging Calibration in 3D Rockfall Modelling. In *Landslide Science and Practice*; Springer: Berlin/Heidelberg, Germany, 2013; pp. 169–175.
37. Kusak, M.; Valagussa, A.; Frattini, P. Key issues in 3d rockfall modeling, natural hazard and risk assessment for rockfall protection in hřensko (Czechia). *Acta Geodyn. Et Geomater.* **2019**, *16*, 393–408. [\[CrossRef\]](#)
38. Pilz, J.; Agliardi, F.; Crosta, G.B.; Zavodni, Z.M. Three-dimensional rock fall simulation in the mining environment using Hy_Stone. In Proceedings of the Slope Stability 2011: International Symposium on Rock Slope Stability in Open Pit Mining and Civil Engineering, Vancouver, BC, Canada, 18–21 September 2011.
39. Depountis, N.; Lainas, S.; Pyrgakis, D.; Sabatakakis, N.; Koukis, G. Engineering geological and geotechnical investigation of landslide events in wildfire affected areas of Ilia Prefecture, Western Greece. *Bull. Geol. Soc.* **2010**, *43*, 1138–1148. [\[CrossRef\]](#)
40. Vagenas, N. Rockfall Simulation by Analytical Methods. Correlation of Rockfall Energy Dissipation Parameters and Rock Mass Characteristics. Ph.D. Thesis, University of Patras, Greece, Department of Geology, Patras, Greece, 2020.
41. Kakavas, M.P.; Nikolakopoulos, K.G.; Kyriou, A.; Koukouvelas, I. The Influence of the DEM Spatial Resolution in Rockfall Simulation and Validation with In Situ Data. *Geosciences* **2023**, *13*, 57. [\[CrossRef\]](#)
42. Jaboyedoff, M.; Labiouse, V. Preliminary estimation of rockfall runout zones. *Nat. Hazards Earth Syst. Sci.* **2011**, *11*, 819–828. [\[CrossRef\]](#)
43. Lanfranconi, C.; Frattini, P.; Sala, G.; Dattola, G.; Bertolo, D.; Sun, J.; Crosta, G.B. Accounting for the effect of forest and fragmentation in probabilistic rockfall hazard. *Nat. Hazards Earth Syst. Sci.* **2023**, *23*, 2349–2363. [\[CrossRef\]](#)
44. Margottini, C.; Spizzichino, D.; Crosta, G.B.; Frattini, P.; Mazzanti, P.; Scarascia Mugnozza, G.; Beninati, L. Rock fall instabilities and safety of visitors in the historic rock cut monastery of Vardzia (Georgia). In *Volcanic Rocks and Soils*; CRC Press: Boca Raton, FL, USA; Balkema: Cape Town, South Africa; Taylor and Francis Group: Abingdon, UK, 2016; pp. 371–378.

45. Crosta, G.B.; Agliardi, F.; Frattini, P. Modelling rockfall impact onstructures. In *Geophysical Research Abstracts*; EGU05-A-08555; H3.01-1WE4P-0110; Copernicus GmbH: Göttingen, Germany, 2005.
46. Crosta, G.B.; Frattini, P.; Imposimato, S.; Agliardi, F. Modeling vegetation and fragmentation effects on rockfalls. *Geophys. Res.* **2006**, *8*, 07694.

Disclaimer/Publisher's Note: The statements, opinions and data contained in all publications are solely those of the individual author(s) and contributor(s) and not of MDPI and/or the editor(s). MDPI and/or the editor(s) disclaim responsibility for any injury to people or property resulting from any ideas, methods, instructions or products referred to in the content.